Received: 6 January 2018 | Revised: 7 February 2018 | Accepted: 12 February 2018

DOI: 10.1002/aoc.4347

FULL PAPER

WILEY Applied Organometallic Chemistry

Azo dye with nitrogen donor sets of atoms and its metal complexes: Synthesis, characterization, DFT, biological, anticancer and Molecular docking studies

Walaa H. Mahmoud[1] | Fatma N. Sayed[1] | Gehad G. Mohamed[1,2]

[1] Chemistry Department, Faculty of Science, Cairo University, Giza 12613, Egypt

[2] Egypt Nanotechnology Center, Cairo University, El-Sheikh Zayed, 6th October 12588, Egypt

Correspondence
Dr. Walaa Hamed Mahmoud, Chemistry Department, Faculty of Science, Cairo University, Giza, 12613, Egypt.
Email: dr.walaa@yahoo.com

An azo derivative was synthesized by coupling diazotized 2,6-diaminopyridine with p-dimethyl amino benzaldehyde and this new ligand formed a series of metal complexes with Cr(III), Mn(II), Fe(III), Co(II), Ni(II), Cu(II), Zn(II) and Cd(II) salts. These complexes were characterized on the basis of elemental analyses, molar conductance, infrared spectroscopy, UV–Vis, ^{1}H NMR, mass spectrometry, electronic spectra, magnetic susceptibility and ESR spectral studies, conductivity measurements, thermogravimetric analyses (TG-DTG). The molecular and electronic structure of the azo ligand was optimized theoretically and the quantum chemical parameters were calculated. The ligand and its metal complexes were subjected to X-ray powder diffraction study. The thermal stability of the ligand and its metal complexes was examined by thermogravimetry. The ligand and its complexes were tested for their in vitro antimicrobial activity, some of the complexes showed good antimicrobial activities against some selected bacterial and fungal strains. Anticancer activity of the ligand and its metal complexes are evaluated against human cancer (MCF-7 cells viability). Molecular docking was used to predict the binding between azo ligand and the receptors of nucleoside diphosphate kinase of *Staphylococcus aureus* (3Q8U) and (3HB5) which is breast cancer mutant oxidoreductase. The docking study provided useful structural information for inhibition studies.

KEYWORDS
azo ligand, MCF-7 cells, molecular docking, quantum chemical parameters, spectroscopy

1 | INTRODUCTION

Azo dyes and pigments constitute by far the most important chemical class of organic colorant owing to their versatile application in various fields of dye and organic chemistry.[1] Azo dyes synthesized from heterocyclic compounds have attracted much attention for their bright and strong color shades ranging from yellow to greenish blue on synthetic and natural fabrics.[1,2]

The great majority of azo dyes are monoazo compounds, which have the common structure unit of the azo chromophore N=N linking two aromatic systems. The textile industry is the largest consumer of dye stuffs. Although some azo dyes have been reported to be toxic, dozens of additional monoazo dyes are permitted in drugs and cosmetics.[3] The oxidation reduction behavior of these compounds play an important role in its biological activity. The pharmaceutical importance of compounds including an aryl azo group has been

extensively reported in the literature.[4] The tautomerism of azo benzene derivatives leads to their applicability as biomarkers and chemical sensors.[5] Because of the good thermal stability of azo compounds, one of the most important applications of azo compounds is in the optical data storage. In general, cyanine dyes, phthalocyanine dyes, and metaleazo complex dyes are used for DVD-R (digital versatile disc-recordable) as recording layer. On the other hand, organic azo compounds and metal-azo complexes are more stable than cyanine dyes against light, provide easier control of the wavelength according to the substituted groups, and have good thermal stability with a metal complex.[6] Because of the importance of azo-containing compounds and in continuance of our interest in syntheses of azo-based compounds,[7] we report herein the syntheses and study of new azo compounds derived from 2,6-diaminopyridine with p-dimethyl amino benzaldehyde and its transition metal complexes.

2 | EXPERIMENTAL

2.1 | Materials and reagents

All chemicals used were of the analytical reagent grade (AR) and of highest purity available. The chemicals used included 2,6-diaminopyridine (Sigma Aldrich, Germany), p-dimethylaminobenzaldehyde (Sigma Aldrich, Germany), $CrCl_3.6H_2O$ (Sigma Aldrich, Germany), $MnCl_2.2H_2O$ (Sigma Aldrich, Germany), $NiCl_2.6H_2O$ (BDH), $FeCl_3.6H_2O$ (Sigma Aldrich, Germany), $CoCl_2.6H_2O$ (Sigma Aldrich, Germany), $CuCl_2.2H_2O$ (Merck, Germany), $CdCl_2$ (Sigma Aldrich, Germany) and $ZnCl_2$ (Strem Chemicals, United States). Organic solvents were spectroscopic pure from BDH included ethanol and dimethyl formamide. Hydrochloric acid, sodium nitrite and sodium acetate (A.R., Sigma Aldrich, Germany) were used.

Human tumor cell line (Breast cell line MCF7) was obtained frozen in liquid nitrogen (-180 °C) from the American Type Culture Collection and was maintained in the National Cancer Institute, Cairo, Egypt, by serial subculturing.

2.2 | Solutions

Stock solutions of metal complexes of $1x10^{-3}$ M were prepared by dissolving the accurately weighed amount of the complexes in DMF for measuring conductivity. Solutions of the azo dye ligand ($1x10^{-5}$ M), its Cr(III), Co(II) and Zn(II) complexes ($1x10^{-4}$ M) and its Mn(II), Fe(III), Ni(II), Cu(II) and Cd(II) complexes ($5x10^{-5}$) were prepared by accurate dilution of the previous prepared stock solutions to measure UV–Vis spectra.

2.3 | Solutions for anticancer activity studies

A fresh stock solution of $1x10^{-3}$ M of azodye ligand (0.00429 g/L) was prepared in the appropriate volume of DMF. Dimethylsulphoxide (DMSO); used in cryopreservation of cells and RPMI-1640 medium was supplied from Sigma. The medium was used for culturing and maintenance of the human tumor cell line. The medium was supplied in a powder form. It was prepared as follows: 10.4 g medium was weighed, mixed with 2 g sodium bicarbonate, completed to 1 l with distilled water and shaked carefully till complete dissolution. The medium was then sterilized by filtration in a Millipore bacterial filter (0.22 μm). The prepared medium was kept in a refrigerator (4 °C) and checked at regular intervals for contamination. Before use, the medium was warmed at 37 °C in a water bath and supplemented with penicillin/streptomycin and FBS. Sodium bicarbonate (Sigma Chemical Co., St. Louis, MO, USA) was used for the preparation of RPMI-1640 medium. 0.05% Isotonic trypan blue solution (Sigma Chemical Co., St. Louis, MO, USA) was prepared in normal saline and was used for viability counting. 10% Fetal Bovine Serum(FBS) (heat inactivated at 56 °C for 30 min), 100 units/ml Penicillin and 2 mg/ml Streptomycin were supplied from Sigma Chemical Co., St. Louis, MO, USA and were used for the supplementation of RPMI-1640 medium prior to use. 0.025% (*w*/*v*) Trypsin (used for the harvesting of cells), 1% (*v*/v) acetic acid (was used for dissolving the unbound SRB dye), 0.4% sulphorhodamine-B (SRB) dissolved in 1% acetic acid was used as a protein dye. Stock solution of trichloro acetic acid (TCA, 50%) was prepared and stored. All of them were supplied from Sigma. 50 μl of the stock solution was added to 200 μl RPMI-1640 medium/well to yield a final concentration of 10% used for protein precipitation. 100% Isopropanol and 70% ethanol were used. Tris base 10 mM (pH 10.5) was used for SRB dye solubilization. 121.1 g of tris base was dissolved in 1000 ml of distilled water and pH was adjusted by HCl (2 M).

2.4 | Measurements

Microanalyses of carbon, hydrogen and nitrogen were carried out at the Microanalytical Center, Cairo University, Egypt, using CHNS-932 (LECO) Vario Elemental Analyzer. Analyses of the metals followed the dissolution of the solid complexes in concentrated HNO_3, neutralizing the diluted aqueous solutions with ammonia and titrating the metal solutions with EDTA. ^1H NMR spectra, as a solution in DMSO-*d6*, were recorded on a 300 MHz Varian-Oxford Mercury at room temperature using TMS as an internal standard. Electron spin resonance spectra

TABLE 1 The different optimized and quantum chemical parameters of free L ligand

Atoms	Bond lengths (Å)	Atoms	Bond lengths (Å)
C1-C2	1.4062	C25-C27	1.4399
C1-C6	1.4136	C25-N33	1.3835
C1-H7	1.0837	C26-C28	1.3989
C2-C3	1.4206	C26-H29	1.087
C2-N11	1.4309	C27-C30	1.3858
C3-C4	1.4017	C27-H31	1.0834
C3-H8	1.0843	C28-C30	1.4232
C4-C5	1.4084	C28-C53	1.4717
C4-H9	1.087	C30-H32	1.087
C5-C6	1.4122	N32-C43	1.476
C5-H10	1.0862	N32-C47	1.475
C6-N12	1.4295	N33-35C	1.4753
N9-N12	1.2939	N33-C39	1.4747
N10-N11	1.2945	C35-H36	1.0977
N11-C15	1.4203	C35-H37	1.0978
N12-C24	1.4222	C35-H38	1.09
C15-C16	1.447	C39-H40	1.0941
C15-C17	1.4154	C39-H41	1.1015
C16-C18	1.4404	C39-H42	1.0949
C16-N32	1.3828	C43-H44	1.0972
C17-C19	1.3983	C43-H45	1.0974
C17-H20	1.087	C43-H46	1.0903
C18-C21	1.3854	C47-H48	1.0939
C18-H22	1.0833	C47-H49	1.1014
C19-C21	1.4236	C47-H50	1.095
C19-C51	1.472	C51-H52	1.1086
C21-H23	1.087	C51-O55	1.2536
C24,-C25	1.4461	C53-H50	1.1088
C24-C26	1.4147	C53-O54	1.2536
The calculated quantum chemical parameters			
E (a.u.)	−1407.61		
Dipole moment (Debye)	6.73		
E_{HOMO} (eV)	−5.71		
E_{LUMO} (eV)	−2.77		
Δ E (eV)	2.94		
χ(eV)	4.24		
η (eV)	1.47		
σ $(eV)^{-1}$	0.68		
Pi (eV)	−4.24		
S $(eV)^{-1}$	0.34		
ω (eV)	6.11		
ΔN_{max}	2.88		

were also recorded on JES-FE2XG ESR spectrophotometer at Microanalytical Center, Tanta University. The X-ray powder diffraction analyses were carried out using Philips Analytical X-ray BV, diffractometer type PW 1840. Radiation was provided by copper target (Cu anode 2000 W) high intensity X-ray tube operated at 40 KV and 25 mA. Divergence and the receiving slits were 1 and 0.2, respectively. Mass spectra were recorded by the EI technique at 70 eV using MS-5988 GS-MS Hewlett–Packard instrument at the Microanalytical Center, National Center for Research, Egypt. FT-IR spectra were recorded on a Perkin-Elmer 1650 spectrometer (4000–400 cm^{-1}) in KBr pellets. The electronic spectra were recorded in DMSO at room temperature on Shimadzu UV–visible mini-1240 spectrophotometer. The molar magnetic susceptibility was measured on powdered samples using the Faraday method. The diamagnetic corrections were made by Pascal's constant and $Hg[Co(SCN)_4]$ was used as a calibrant. Molar conductivities of 10^{-3} M solutions of the solid complexes in DMF were measured using Jenway 4010 conductivity meter. The thermogravimetric analyses (TG and DTG) of the solid complexes were carried out from room temperature to 1000 °C using a Shimadzu TG-50H thermal analyzer. Diffused reflectance spectra analyses were carried out at the Microanalytical Center, Cairo University, Egypt. The antimicrobial activities were carried out at the Microanalytical Center, Cairo University, Egypt. The anticancer activity was performed at the National Cancer Institute, Cancer Biology Department, Pharmacology Department, Cairo University. The optical density (O.D.) of each well was measured spectrophotometrically at 564 nm with an ELIZA microplate reader (Meter tech. R 960, USA).

2.5 | Synthesis of azodye ligand

In 250 ml quickfit round bottom flask, 2,6-diaminopyridine (3.00 g, 27.30 mmol) was dissolved in ethanol (50 ml). The solution was cooled with stirring in an ice bath to 0 °C until it becomes clear, then HCl solution (4 ml) was added. Solution of sodium nitrite (3.76 g, 54.50 mmol) in distelled water (20 ml) was added dropwise during 10 min and the reaction mixture was further stirred for 20 min in an ice bath at 0-5 °C. The solution was added dropwise to p-dimethylaminobenzaldehyde coupling component (8.10 g, 54.50 mmol) in ethanol (30 ml) and aqueous solution of 4 g sodium acetate as catalyst, with stirring in an ice bath for a further 1 h. The product was collected by filtration and washed with water and dried under vacuum at room temperature. The physical and analytical data of the isolated azodye ligand are listed in Table 3. The compound has high melting point and it is found to be air stable.

2.6 | Synthesis of metal complexes

Azodye ligand was dissolved in DMF (0.4 g, $9.32x10^{-4}$ mmol) and ethanolic metal salts with the same molar ratio (0.248 g Cr(III), 0.184 g Mn(II), 0.252 g Fe(III), 0.222 g Co(II), 0.220 g Ni(II), 0.125 g Cu(II), 0.127 g Zn(II) and 0.171 Cd(II)) were added to the azo ligand solution. The mixture was heated under reflux for 2–3 h with stirring. The precipitates were filtered off, washed with ethanol followed by diethyl ether and dried in a vacuum desiccator over anhydrous $CaCl_2$.

2.7 | Spectrophotometric studies

The absorption spectra were recorded for $1x10^{-5}$ M solutions of the azodye free ligand, $1x10^{-4}$ M solutions of its Cr(III), Co(II) and Zn(II) metal complexes and $5x10^{-5}$ M solutions of its Mn(II), Fe(III), Ni(II), Cu(II) and Cd(II) metal complexes dissolved in DMF. The spectra were scanned within the wavelength range from 200 to 700 nm.

2.8 | Pharmacology

2.8.1 | Antimicrobial activity

A filter paper disk (5 mm) was transferred into 250 ml flasks containing 20 ml of working volume of tested solution (100 mg/ml). All flasks were autoclaved for 20 min at 121 °C. LB agar media surfaces were inoculated with four investigated bacteria (Gram positive bacteria: *Bacillus subtilis* and *Staphylococcus aureus*, Gram negative bacteria: *Neisseria gonorrhoeae* and *Escherichia coli*) and one strain of fungi (*Candida albicans*) by diffusion agar technique, then, transferred to a saturated disk with a tested solution in the center of Petri dish (agar plates). All the compounds were placed at 4 equidistant places at a distance of 2 cm from the center in the inoculated Petriplates. DMSO served as control. Finally, all these Petri dishes were incubated at 25 °C for 48 h where clear or inhibition zones were detected around each disk. Control flask of the experiment was designed to perform under the same condition described previously for each microorganism but with dimethylformamide solution only and by subtracting the diameter of inhibition zone resulting with dimethyl formamide from that obtained in each case, so antibacterial activity could be calculated.[8,9] Amikacin and ketoconazole were used as reference compounds for antibacterial and antifungal activities, respectively. All experiments were performed as triplicate and data plotted were the mean value.

2.9 | Anticancer activity

Potential cytotoxicity of the complexes was tested using the method of Skehan and Storeng.[8,10] Cells were plated in 96-multiwell plate (104 cells/well) for 24 h before treatment with the complexes to allow attachment of cell to the wall of the plate. Different concentrations of the complexes under investigation (0, 5, 12.5, 25, 50 and 100 μg/ml) were added to the cell monolayer triplicate wells were prepared for each individual dose. The monolayer cells were incubated with the complexes for 48 h at 37 °C and in 5% CO_2 atmosphere. After 48 h, cells were fixed, washed and stained with SRB stain. Excess stain was washed with acetic acid and attached stain was recovered with tris–EDTA buffer. The optical density (O.D.) of each well was measured spectrophotometrically at 564 nm with an ELIZA microplate reader and the mean background absorbance was automatically subtracted and mean values of each drug concentration was calculated. The relation between surviving fraction and drug concentration is plotted to get the survival curve of Breast tumor cell line for each complex.

Calculation:

The percentage of cell survival was calculated as follows:

$$\text{Survival fraction} = \text{O.D.(treated cells)}/\text{O.D.(control cells)}.$$

The IC_{50} values (the concentrations of the azo ligand or its complexes required to produce 50% inhibition of cell growth). The experiment was repeated three times for MCF7 cell line.

2.10 | Computational methodology

The electronic structure calculations of azo ligand were carried out using the Gaussian03 suite of program.[11] They were fully optimized employing DFT based B3LYP method along with the LANL2DZ basis set. In order to incorporate the effect of the solvent around the molecule, the TD-DFT method (along with LANL2DZ basic set) was used to calculate the electronic absorption spectra of the azo ligand. The contribution of molecular orbital on HOMO and LUMO was also calculated.

2.11 | Molecular docking

In order to find out the possible binding modes of the most active compounds against the receptors of nucleoside diphosphate kinase of *Staphylococcus aureus* (3Q8U) and (3HB5) which is breast cancer mutant oxidoreductase. The molecular docking studies were performed using MOE 2008 software and it is rigid molecular docking software[12] and is an interactive molecular graphics program for calculating and displaying feasible docking modes of a receptor and ligand and complex molecules. It necessitates the ligand and the receptor as input in PDB format. The amino acid chain was kept and the water molecules and co-crystallized ligands were removed. The structure of ligand in PDB file format was created by Gaussian03 software. The crystal structures of receptors (3Q8U) and (3HB5) were downloaded from the protein data bank (http://www.rcsb.org./pdb).

3 | RESULTS AND DISCUSSION

3.1 | Characterization of azodye ligand

Free ligand and its metal complexes are soluble in DMF and DMSO solvents and have high and sharp melting points which indicate their pure nature. The infrared spectrum of azo ligand (L) gives interesting results and conclusions, the most effective bands are listed in Table 4. The frequency for the N=N stretching laid in the region 1542 cm^{-1},[13] also two bands are observed due to vibrational ν(C=N) mode of pyridine ring at 1596 cm^{-1} and the ν(C=O) frequency in the free L at 1665 cm^{-1}. [14] The IR spectrum of the ligand also showed a sharp band at 1162 cm^{-1} due to vibration of υ($N(CH_3)_2$), also three bands were observed due to υ(C-N) stretching and δ(C=N) bending at 1475 $cm^{-1}$and 631 $cm^{-1,}$ respectively.

^{1}H NMR spectrum of free ligand (L) in DMSO-d_6 show three characteristic signals at:

3.03 ppm (s, 12H, CH_3) and 9.66 ppm (s, 2H, CHO) assigned to $N(CH_3)_2$ and aldehydic groups, respectively.[15] In the aromatic region, a few doublets and in few cases some overlapping multiplets are observed in the range δ (6.76–7.68) ppm. These multiplets are due to pyridine ring and aryl protons.[13] From the mass spectrometry data, the azodye ligand shows molecular ion peak at m/z = 428 amu which was in close agreement with expected molecular weight at 429 g/mol.

3.2 | Geometry optimization

The optimized structures of the azo ligand (L) were calculated using the Gaussian03 suite of program. [11] They were fully optimized employing DFT based B3LYP method along with the LANL2DZ basis set. Table 1 shows some selected geometric parameters from the optimized structure. Figure 1 illustrates the optimized structure of azo ligand (L). The HOMO and LUMO of L is shown in Figure 2. The HOMO–LUMO energy gap, ΔE, which is an important stability index, is applied to develop theoretical models for explaining

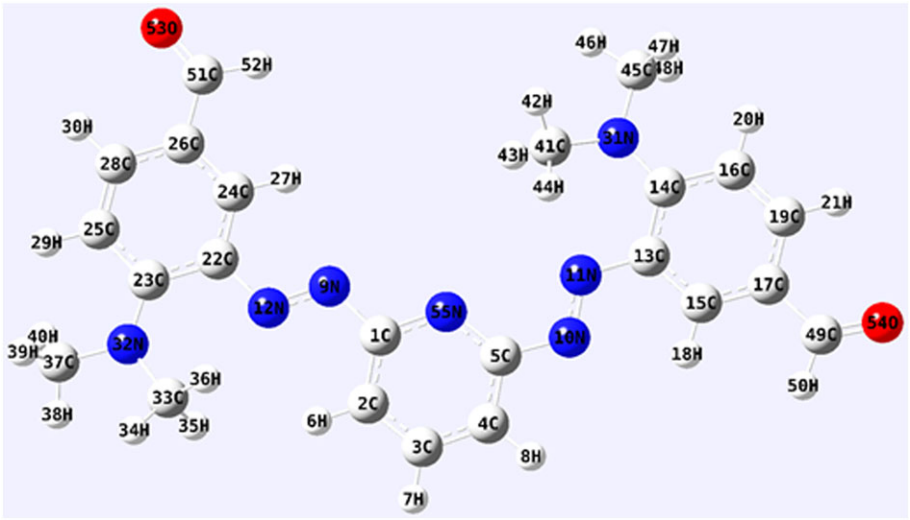

FIGURE 1 The optimized structure of the free ligand (L)

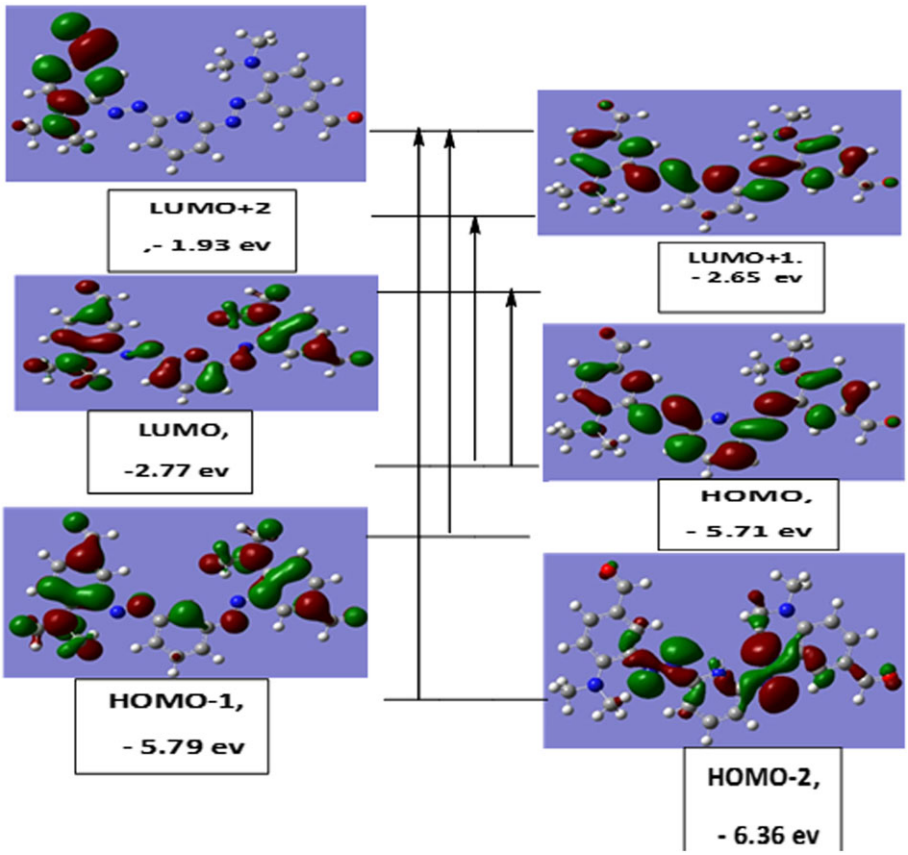

FIGURE 2 Theoretical electronic absorption transitions for L in DMF solvent

the structure and conformation barriers in many molecular systems.[16,17]

The calculated quantum chemical parameters are given in Table 1. Additional parameters such as ΔE, absolute electronegativities, χ, chemical potentials, Pi, absolute hardness, η, absolute softness, σ, global electrophilicity, ω, global softness, S, and additional electronic charge, ΔN_{max}, have been calculated according to the following equations:[18–20]

$$\Delta E = E_{LUMO} - E_{HOMO} \quad (1)$$

$$\chi = \frac{-(E_{HOMO} + E_{LUMO})}{2} \quad (2)$$

$$\eta = \frac{E_{LUMO} - E_{HOMO}}{2} \quad (3)$$

$$\sigma = \frac{1}{\eta} \quad (4)$$

$$Pi = -\chi \quad (5)$$

$$S = \frac{1}{2\eta} \quad (6)$$

$$\omega = \frac{Pi^2}{2\eta} \quad (7)$$

$$\Delta N_{\max} = -\frac{Pi}{\eta} \quad (8)$$

3.3 | Electronic spectra and frontier molecular orbital energies

The UV–Vis electronic spectra of L in DMF were recorded at the range of 700–200 nm. The theoretical electronic absorption wavelengths and oscillator strengths were calculated by the TD-DFT method with B3LYP /LanL2DZ basis sets in above solvent. Obtained theoretical results are summarized along with the experimental ones in Table 2. The data shows that there are two absorption bands at 255 and 388 nm in DMF solvent. The corresponding peaks in TD-DFT calculations are found at the range of 253, 337, 493 and 533 nm in DMF solvent as can be seen in Table 5. The patterns of highest occupied (HOMO) and the lowest unoccupied molecular orbitals (LUMO) have been given in Figure 2. While LUMO represents the ability to obtain an electron, HOMO represents the ability to donate an electron. In other words, the energy of the HOMO is directly related to the ionization potential, LUMO energy is directly related to the electron affinity. Hence these frontier energies play an important role in the electric and optical properties as well as energies is a critical parameter in determining molecular electrical transport properties due to providing measurement of electron conductivity. In addition, this energy gap characterizes the molecular stability and spectroscopic properties of the molecular systems. The smaller energy gap describes chemically soft molecule which can be easily polarizable. The energy gap of L was calculated at 2.94 eV by TD-DFT level.

3.4 | Characterization of metal complexes

3.4.1 | Elemental analyses:

The elemental analysis data of the complexes (Table 3) show the formation of the complexes in the ratio of 1:1 for [ML]. It is found that the theoretical values are in agreement with the found values. The metal complexes have high melting points and they are found to be air stable. The azodye ligand is soluble in common organic solvents and all the complexes are freely soluble in DMF and DMSO but insoluble in methanol, ethanol and water.

3.4.2 | Molar conductance measurements:

The conductivity data in DMF are in the range reported for 2:1 and 1:1 electrolytes. The complexes of $[Cr(L)Cl]Cl_2.2H_2O$, $[Mn(L)H_2O]Cl_2$, $[Fe(L)Cl]Cl_2.H_2O$ and $[Cu(L)H_2O]Cl_2.H_2O$ have values indicate that they are 2:1 electrolytes and other complexes are 1:1 electrolytes [21].

3.5 | IR spectral studies

IR spectral study has proven to be the most suitable technique to give enough information to elucidate the way of bonding of ligand to the metal ions Table 4. The bands arising due to υ(C=N) pyridine stretching at 1596 cm^{-1}[21] which shifted to 1591–1602 cm^{-1}, υ(N=N) at 1542 cm^{-1} was observed to be shifted to 1537–1540 cm^{-1}[22] and the $\upsilon(N(CH_3)_2)$ stretching frequency in the free ligand at 1162 cm^{-1} that showed shift to 1160–1174 cm^{-1} in the metal complexes indicating the involvement of nitrogen of pyridine ring, nitrogen of the azo group and nitrogen of amino group in the complex formation. The band was observed at 1665 cm^{-1} assigned to υ(C=O) stretching frequency showed very little changes at 1660–1664 cm^{-1} which indicated to non-contribution of carbonyl group in

TABLE 2 Main calculated optical transition with composite ion in terms of molecular orbital

Compound	Transition	Excitation energy (ev)	λ_{max} Calc. (nm)	λ_{max} exp. (nm)	Oscillating strength
L	HOMO → LUMO	2.94	533	.....	0.01
	HOMO → LUMO+1	3.06	493	.....	0.71
	HOMO-1 → LUMO+2	3.86	337	388	0.05
	HOMO-2 → LUMO+2	4.43	253	255	0.20

TABLE 3 Analytical and physical data of L and its metal complexes

Compound (Molecular Formula)	Colour (%yield)	M.p. (°C)	% Found (Calcd.)					$\mu_{eff.}$ (B.M.)	$\Lambda_m\ \Omega^{-1}\ mol^{-1}\ cm^2$
			C	H	N	Cl	M		
L ($C_{23}H_{23}N_7O_2$)	Green (90)	76	64.71 (64.34)	5.41 (5.36)	22.57 (22.84)	-----	-----	-----	-----
[Cr(L)Cl]Cl_2.2H_2O ($C_{23}H_{27}Cl_3CrN_7O_4$)	Brown (87)	230	46.09 (44.38)	4.68 (4.33)	16.73 (15.72)	17.22 (17.59)	8.88 (8.59)	3.84	118
[Mn(L)H_2O]Cl_2 ($C_{23}H_{25}Cl_2MnN_7O_3$)	Dark brown (88)	>300	47.70 (48.17)	4.61 (4.36)	17.21 (17.10)	12.66 (12.39)	9.32 (9.60)	5.41	142
[Fe(L)Cl]Cl_2.H_2O ($C_{23}H_{25}Cl_3FeN_7O_3$)	Dark brown (80)	100	46.30 (46.66)	3.78 (3.89)	16.35 (16.57)	17.86 (18.01)	9.06 (9.47)	5.34	128
[Co(L)Cl]Cl.H_2O ($C_{23}H_{25}Cl_2CoN_7O_3$)	Dark brown (85)	230	47.60 (47.83)	3.91 (4.33)	17.04 (16.98)	12.74 (12.31)	10.56 (10.23)	5.22	86
[Ni(L)Cl]Cl.H_2O ($C_{23}H_{25}Cl_2NiN_7O_3$)	Brown (86)	114	48.28 (47.86)	4.49 (4.34)	17.28 (16.99)	11.98 (12.31)	10.34 (10.18)	3.22	81
[Cu(L)H_2O]Cl_2.H_2O ($C_{23}H_{27}Cl_2CuN_7O_4$)	Dark brown (89)	>300	47.90 (47.46)	4.06 (4.30)	17.26 (16.85)	12.59 (12.21)	11.21 (10.92)	1.76	113
[Zn(L)Cl]Cl.H_2O ($C_{23}H_{25}Cl_2ZnN_7O_3$)	Dark brown (91)	270	47.23 (47.34)	4.65 (4.29)	17.05 (16.81)	11.87 (12.18)	11.46 (11.15)	Diam.	66
[Cd(L)Cl]Cl ($C_{23}H_{23}Cl_2CdN_7O_2$)	Brown (82)	230	44.77 (45.07)	3.75 (3.76)	16.47 (16.00)	11.76 (11.59)	18.62 (18.35)	Diam.	73

TABLE 4 IR spectra (4000–400 cm^{-1}) of L and its metal complexes

L	[Cr(L) Cl]Cl_2.2H_2O	[Mn(L)H_2O]Cl_2	[Fe(L)Cl]Cl_2.H_2O	[Co(L)Cl]Cl.H_2O	[Ni(L)Cl]Cl.H_2O	[Cu(L)H_2O]Cl_2.H_2O	[Zn(L)Cl]Cl.H_2O	[Cd(L)Cl]Cl	Assignment
1665sh	1664 m	1660w	1660w	1660s	1660s	1661s	1660w	1664 m	CO stretching
1596 sh	1597 m	1598sh	1592sh	1591sh	1602sh	1591sh	1592 m	1598s	C=N Pyridine stretching
1542sh	1539 m	1537 m	1540s	1538 m	1540s	1537 m	1540s	1540 m	N=N
1475 m	1436 m	1441 s	1440 w	1438 s	1441 m	1435 s	1438 w	1437 m	C-N stretching
1162sh	1160 m	1174 m	1173 m	1172 m	1166sh	1170 m	1172 m	1160s	$N(CH_3)_2$
1065 m	1065s	1061s	1055s	1056s	1063s	1060w	1060w	1066 m	Pyridine ring stretching
631sh	590 m	607 m	599 m	599 s	676 s	630 s	620w	622 m	δ(C=N)
---------	----------	943w,815 m	----------	----------	----------	950 s,820 m	----------	---------	H_2O stretch of coordinated water
----------	--------	520 s	----------	----------	----------	520 s	----------	----------	M-O stretch of coordinated water
----------	463w	490w	495w	424 s	470 s	463w	442 s	442 s	M-N

sh = sharp, m = medium, br = broad, s = small, w = weak

the coordination.[23] Also new bands were observed at 939–960 cm^{-1} and 815–821 cm^{-1} due to H_2O stretch of coordinated water in Mn(II), Cu(II) and Zn(II) complexes and new bands at 518–522 cm^{-1} due to M-O stretch of coordinated water in the same complexes. IR spectrum showed a new band at the region 424–495 cm^{-1} assigned to υ(M-N).[24]

3.6 | ^{1}H NMR spectral studies

^{1}H NMR spectral data in DMSO solution of the ligand, Zn(II) and Cd(II) complexes showed that the resonance of protons has been assigned on the basis of their integration and multiplicity pattern. ^{1}H NMR spectrum of the ligand reveals the following signals at:

δ = 9.66 ppm (s, 2H, CHO), 6.76–7.68 ppm (m, 9H, pyridine ring and two benzene rings) and 3.03 ppm (s, 12H, CH_3).[25]

While, the ^{1}H NMR spectrum of Zn(II) reveals the following signals at δ = 9.64 (s, 2H, CHO), 6.75–7.67 (m, 9H, pyridine ring) and 3.02 (s, 12H, CH_3) and spectrum of Cd(II) complex showed signals at δ = 9.64, 9.63 (s, 2H, CHO), 6.75–7.67 (m, 9H, pyridine ring) and 3.02, 3.03 (s, 12H, CH_3). This shifting indicated that metal complexes were formed by binding of metal ion with $N(CH_3)_2$, nitrogen of pyridine ring and azo group.

3.6.1 | Mass spectral studies:

The electronic mass spectrum of Fe(III) and Ni(II) complexes confirm formation of these complexes by showing molecular ion peaks at m/z = 606 and 575, respectively, which are very close to expected molecular weight which were 610 g/mol for Fe(III) and 577 g/mol for Ni(II) and also show peaks at m/z = 430, 432 amu, respectively, indicates to the ligand. The intensities of these peaks show the stabilities of the complexes.

3.6.2 | UV–Vis absorption studies:

UV–visible spectral data of the free ligand shows absorption bands at 338 and 255 nm corresponding to n → π* transitions and π → π* transitions of C=O, heterocyclic moieties and benzene ring, respectively.

In the spectra of metal ions complexes these bands are shifted to higher or lower frequencies where the n → π* transition bands are shifted to 397–308 nm in all complexes and π → π* transition bands are shifted to 268–251 nm in Mn(II), Co(II), Ni(II), Zn(II) and Cd(II), while disappeared in Cr(III), Fe(III) and Cu(II) indicating that the ligands coordinate to metal ions.[26,27]

3.6.3 | Electronic spectra and magnetic moment measurements:

For the hexa-coordinate Cr(III) complex, its diffused reflectance spectrum exhibits three absorption bands at 21,980, 19,444 and 17,310 cm^{-1} which can be assigned to the three spins allowed transitions $^4A_2g(F) \rightarrow {}^4T_1g(P)$, $^4A_2g(F) \rightarrow {}^4T_2\,g(F)$ and $^4A_2g(F) \rightarrow {}^4T_1g(F)$. The electronic spectrum of the chelate reported here is in reasonable agreement with those in the literature. The magnetic moment at room temperature is 3.84 B.M. which corresponds to the expected value for octahedral Cr(III) complexes.[28]

The diffused reflectance spectrum of Mn(II) complex has transition bands at 26,101, 21,730 and 17,910 cm^{-1} which correspond to charge transfer (LMCT), $^6A_{1g} \rightarrow T_{2g}(G)$ and $^6A_{1g} \rightarrow {}^5T_{1g}$, respectively, indicating the octahedral geometry. The magnetic moment value of the Mn(II) complex is 5.64 B M, normally observed for octahedral coordination geometry.[29]

The diffused reflectance spectrum of Fe(III) complex exhibits three bands at 21,740, 19,860 and 16,120 cm^{-1} which may be assigned to $^4T_{2g}(G) \rightarrow {}^6A_{1g}$, $^4T_{2g}(G) \rightarrow {}^6A_{1g}$ and $^4T_{1g}(D) \rightarrow {}^6A_{1g}$ transitions, respectively. The magnetic moment value is found to be 5.32 B.M. which indicates the presence of Fe(III) complex in octahedral geometry.[30,31]

The Co(II) chelate showed two bands at 22,211 and 19,435 cm^{-1} which can be assigned to $^4T_{1g}(F) \rightarrow {}^4T_{2g}\,(P)$ and $^4T_{1g}(F) \rightarrow {}^4A_{2g}(F)$ transitions, respectively, which suggests an octahedral geometry.[26] The magnetic susceptibility measurement lies at 5.10 B.M. which is an indicative of octahedral geometry.

The diffused reflectance spectrum of the Ni(II) complex exhibits transition bands at 27,125, 20,185 and 12,587 cm^{-1} indicating that the Ni(II) complex is octahedral. The room temperature magnetic moment of Ni(II) complex (3.147 B.M.), corresponding to two unpaired electrons and in the range of octahedral Ni(II) complexes.[30–33]

The magnetic moment value for the Cu(II) complex recorded at room temperature is 1.75 B.M. (Table 1) and corresponding to one unpaired electron. The electronic spectrum of the Cu(II) complex gave a band at 17,985 cm^{-1}, suggesting the existence of a transition from d_{xy}, d_{z2} and d_{xz}, d_{yz} transfer to the antibonding and half-filled d_{x2-y2} level which is consistent with an octahedral configuration.[34] The Zn(II) and Cd(II) complexes are diamagnetic. According to the empirical formulae, an octahedral geometry was suggested for these metal chelates.

3.6.4 | ESR studies:

The ESR spectrum of the Cu(II) complex was recorded in DMSO at 300 and 77 K and its parameters and showed

that the observed order for Cu(II) complex ($A_{||}$ (197) > $A_{\perp}$ (98.88); $g_{||}$ (2.04) > $g_{\perp}$ (1.87) indicates that the complex exerts an octahedral geometry.[19] The observed value of G for the Cu(II) complex (G = 1.337) implies that the exchange coupling is not present and misalignment is appreciable. The trend $g_{||} > g_{\perp} >$ ge (2.0023) shows that the unpaired electron is localized in the dx^2- y^2 orbital of the Cu(II) ion in complex.[17,31,35] The g_{iso} (2.04) value less than 2.3 indicates the covalent character of the metal ligand bond and the α^2 value (1.87) suggestive of in-plane covalency. The calculated value ($g_{||}/A_{||}$) 124 cm^{-1} for the complex is consistent with slightly distorted structure and showed poor in-plane π bonding.[36–39]

3.7 | Powder X-ray diffraction spectroscopy

The average crystallite size (ξ) can be calculated from the XRD pattern according to Debye–Scherrer equation

$$\xi = \frac{K\lambda}{\beta_{1/2}\cos\theta}$$

The equation uses the reference peak width at angle (θ), where λ is wavelength of X-ray radiation (1.541874 Å), K is constant taken as 0.95 for organic compounds and $\beta_{1/2}$ is the width at half maximum of the reference diffraction peak measured in radians. The dislocation density,δ, is the number of dislocation lines per unit area of the crystal. The value of δ is related to the average particle diameter (ξ) by the relation:[8,9,40]

$$\delta = \frac{1}{\xi^2}.$$

The values of ξ (2.92–2.93 mm) and δ (0.116–0.117 mm^{-2}) indicated that the ligand and Cr(III) and Ni(II) complexes have crysslline nature while other complexes showed amorphous nature.

3.7.1 | Thermal analysis studies:

The thermal stability of the complexes was investigated using TGA (Figure 3). The thermogravimetric analysis (TGA) data (Table 5) were obtained at a heating rate of 10 °C/min in a nitrogen atmosphere over a temperature range of 20–1000 °C. The free ligand decomposed completely leaving no residues in one step at the temperature range 70-400 °C. Decomposition of Cr(III) complex occurred in five steps. The first step occurred in the temperature range 35-150 °C with maximum temperature 51 °C due to loss of H_2O and $^3/_2Cl_2$ molecules, the second step occured within the temperature range of 150-320 °C with Ts 184 °C corresponding to loss of $C_{16}H_{14}N_4$ and the last three steps occurred within temperature range 320-980° C with maximum temperatures at 351, 636 and 898 °C due to loss of $C_7H_9N_3$ and $^1/_4O_2$ leaving $^1/_2Cr_2O_3$ as a residue. The TG curve of $[Mn(L)H_2O]Cl_2$ showed decomposition through six steps, the first and second steps ocurred within temperature range 35–190 °C with maximum temperatures 152 °C and 187 °C due to loss of H_2O and ½Cl_2 molecules. The third step ocurred

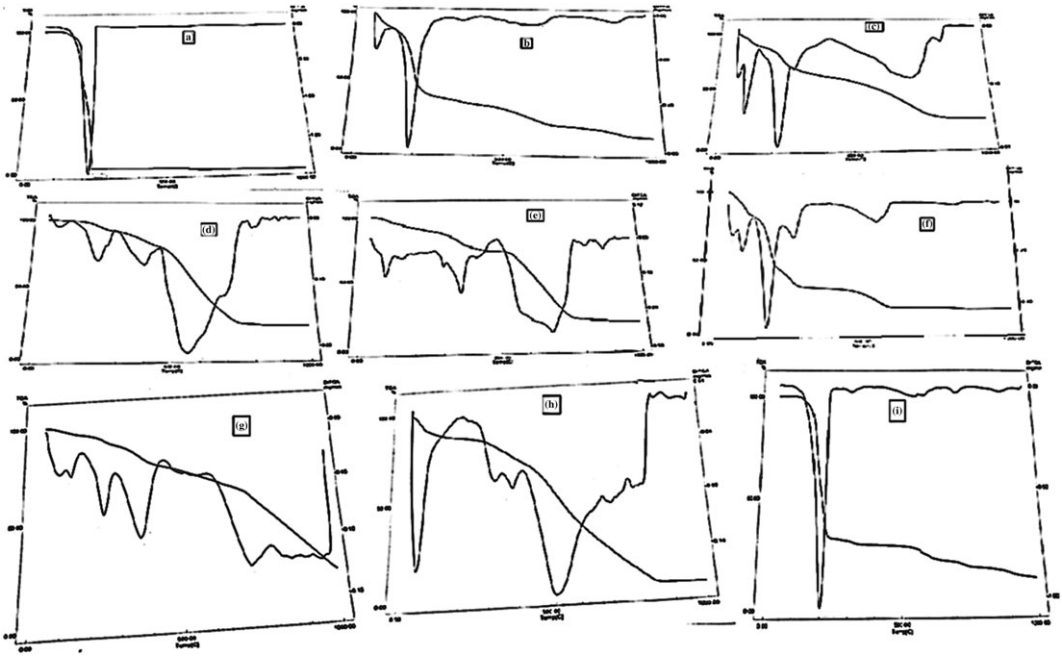

FIGURE 3 Thermal analyses (TG and DTG) of (a) L, (b) Cr(III), (c) Mn(II), (d) Fe(III), (e) Co(II), (f) Ni(II), (g) Cu(II), (h) Zn(II) and (i) Cd(II) complexes

TABLE 5 Thermoanalytical results (TG and DTG) of L and its metal complexes

Complex	TG range (°C)	DTG_{max} (°C)	n*	Mass loss Total mass loss Estim (Calcd) %	Assignment	Residues
L	70–400	221	1	99.9 (100)	-Loss of $C_{23}H_{23}N_7O_2$.	--------
$[Cr(L)Cl]Cl_2.H_2O$	35–150	51	1	19.5 (20.5)	-Loss of H_2O and $^3/_2Cl_2$.	$^1/_2Cr_2O_3$
	150–320	184	1	44.5 (43.3)	-Loss of $C_{16}H_{14}N_4$.	
	320–980	351, 636, 898	3	25.3 (23.6) 87.3 (87.1)	-Loss of $C_7H_9N_3$ and $^1/_4O_2$.	
$[Mn(L)H_2O]Cl_2$	35–190	152, 187	2	11.6 (12.1)	-Loss of H_2O, ½Cl_2 and CH_4.	MnO + 5C
	190–260	218	1	19.9 (18.2)	-Loss of $C_4H_{12}N_2O$.	
	260–1000	265, 719, 851	3	45.4 (46.8) 77.2 (77.3)	-Loss of $C_{13}H_7N_5Cl$.	
$[Fe(L)Cl]Cl_2.H_2O$	30–197	64	1	3.6 (3.0)	.-Loss of H_2O.	½Fe_2O_3 + 3C
	198–485	220, 394	2	21.2 (22.0)	-Loss of $^3/_2Cl_2$ and CO.	
	486–890	555, 813	2	53.8 (53.3) 78.8 (80.97)	-Loss of $C_{16}H_{23}N_7$.	
$[Co(L)Cl]Cl.H_2O$	30–210	85	1	9.9 (9.3)	-Loss of H_2O and ½Cl_2.	CoO + 3C
	210–350	294	1	8.9 (8.8)	-Loss of ½Cl_2 and CH_3.	
	350–950	357, 685, 894	3	62.8 (62.7) 82.0 (80.8)	-Loss of $C_{19}H_{20}N_7O_2$.	
$[Ni(L)Cl]Cl.H_2O$	30–165	52, 90	2	30.1 (31.0)	-Loss of Cl_2, H_2O and $C_4H_{14}N_2$.	NiO + 3C
	165–255	184	1	33.7 (33.1)	- Loss of $C_{12}H_5N_3$.	
	255–900	261, 549, 834	3	22.4 (21.5) 80.7 (80.8)	-Loss of $C_4H_4N_4O$.	
$[Cu(L)H_2O]Cl_2.H_2O$	40–205	80, 129	2	5.9 (6.0)	-Loss of $2H_2O$.	CuO + 4C
	205–355	240	1	10.7 (11.8)	-Loss of Cl_2.	
	355–1000	362, 723	2	62.0 (61.0) 79.0 (78.7)	-Loss of $C_{19}H_{23}N_7O$.	
$[Zn(L)Cl]Cl.H_2O$	35–130	62	1	11.6 (11.9)	-Loss of H_2O, ½Cl_2 and CH_4.	ZnO
	130–340	321	1	9.5 (8.8)	-Loss of ½Cl_2 and CH_4.	
	340–770	380, 519, 683	3	64.4 (63.1) 86.0 (86.1)	-Loss of $C_{21}H_{15}N_7O$.	
[Cd(L)Cl]Cl	30–270	202	1	69.4 (69.2)	-Loss of Cl_2 and $C_{21}H_{15}N_7$.	CdO
	270–630	316, 568, 602	3	8.2 (7.6) 79.6 (79.7)	-Loss of C_2H_8O.	

n* = number of decomposition steps

within temperature range 190–260 °C with Ts 218 °C with mass loss corresponding to and $C_4H_{12}N_2O$. The last three steps occurred within temperature range 260-1000 °C with maximum temperatures 265, 719, 851 °C due to loss of $C_{13}H_7N_5Cl$ leaving MnO contaminated with carbon atoms as residues.

The thermal decomposition of $[Fe(L)Cl]Cl_2.H_2O$ complex proceeded via five degradation steps. The first step occurred within temperature range 30-197 °C with maximum temperature 64 °C due to loss of water molecule, the second and third steps of decomposition occurred within temperature range 198-486 °C at Ts 220 and 394 °C due to loss of $^3/_2$ Cl_2 and CO gases and finally the last two steps occurred within temperature range 487-1000 °C corresponding to loss of $C_{16}H_{23}N_7$ leaving ½Fe_2O_3 + 4C residues. The TG curve of Co(II) complex showed five decomposition steps of the complex. The first step of decomposition occurred in the range of temperature 30-210 °C at Ts 85 °C due to loss of water molecule and chloride atom. The second step occurred within temperature range from 210 °C to 350 °C with maximum temperature 294 °C. The last three steps occurred within the range 350-950 °C with maxima 357, 685 and 894 °C leaving contaminated cobalt oxide.

The $[Ni(L)Cl]Cl.H_2O$ complex is thermally decomposed through six successive decomposition steps. The first two steps occurred in the range 30-165 °C with maxima temperatures 52 and 90 °C may be attributed to the loss of Cl_2, H_2O and $C_4H_{14}N_2$. The third step occurred at 165-255 °C with Ts 184 °C due to loss of $C_{12}H_5N_3$. Finally the last three steps of decompositions occurred within temperature range 255-900 °C with maxima 261, 549 and 834 °C due to loss of $C_4H_4N_4O$ leaving NiO + 3C.

For $[Cu(L)H_2O]Cl_2.H_2O$ complex the TG curve showed mass loss in the temperature range of 40–205 °C associated with one DTG peak at 129 °C. This step can be assigned to loss of two water molecules in one step. The second step occurred within range 205–355 °C with DTG_{max} 240 °C due to mass loss corresponded to chlorine gas. On further heating, the DTG registered peaks at 362 °C and 723 °C within the temperature range of 355–1000 °C that may correspond to loss of remaining ligand fragment ($C_{19}H_{23}N_7O$) leaving CuO contaminated with carbon atoms as a residue. The TG curve of [Zn(L)Cl]Cl.

H_2O complex showed thermal decomposition peak within temperature range 35–130 °C with Ts 62 ° C due to one step of decomposition corresponded to loss of H_2O, ½Cl_2 and CH_4 molecules. The second step occurred within range of 130–340 °C with maximum temperature 321 °C due to loss of ½Cl_2 and CH_4 molecules. The last three steps occurred at 340-770 °C with maxima 380, 519 and 683 °C due to loss of the remaining complex leaving ZnO a residue.

The [Cd(L)Cl]Cl complex is thermally decomposed in four successive decomposition steps. The first step occurred within 30-270 °C with DTG_{max} 202 °C, mass loss corresponding to Cl_2 and $C_{21}H_{15}N_7$. The other three steps occurred in the range from 270 °C to 630 °C with maxima 316, 568 and 602 °C due to loss of the remaining ligand leaving CdO residue.

3.8 | Calculation of activation thermodynamic parameters

The kinetic parameters such as enthalpy of activation (ΔH*), activation energy (ΔE*), free energy change of the decomposition (ΔG*), and entropy of activation (ΔS*) were evaluated graphically by employing the Coats–Redfern[35] and Horowitz–Metzger models equations.[41] The data are summarized in Table 6.

(a) *Coats-Redfern equation*

The Coats-Redfern equation which is a typical integral method, can be represented as:

$$\int_0^{\alpha} \left(d\alpha/(1-\alpha)^n = (A/\alpha)\int_{T1}^{T2} \exp^{(-E^*/RT)dt}\right.$$

For convenience of integration, the lower limit T_1 is usually taken as zero. This equation on integration gives: For convenience of integration, the lower limit T_1 is usually taken as zero. This equation on integration gives:

$$\ln\left[-\ln(1-\alpha)/T^2\right] = \left(-E^*/RT\right) + \ln\left[AR/\varphi E^*\right]$$

A plot of left-hand side (LHS) against 1/T was drawn, E* is the energy of activation in kJ mol^{-1} and calculated from the slope and A in (s^{-1}) from the intercept. The entropy of activation ΔS* in (J K^{-1} mol^{-1}) was calculated by using equation:

$$\Delta S^* = R\ \ln\left(Ah/K_B T_s\right)$$

TABLE 6 Thermodynamic data of the thermal decomposition of L and its metal complexes

Complex	Decomp.Temp. (°C)	E* (kJmol^{-1})	A (s^{-1})	ΔS* (KJmol^{-1})	ΔH* (kJmol^{-1})	ΔG* (kJmol^{-1})
L	70–400	110.9 (124.3)	2.66x10^{11} (1.64x10^{11})	−18.60 (−22.80)	110.5 (123.9)	183.0 (191.0)
[Cr(L)Cl]Cl_2.2H_2O	35–150	18.29 (18.39)	8.75x10^{9} (6.87x10^{9})	−52.90 (−54.60)	68.27 (68.36)	94.0 (96.80)
	150–320	21.90 (21.71)	5.25x10^{8} (1.96x10^{8})	−44.10 (−45.20)	91.86 (91.67)	137.0 (140.0)
[Mn(L)H_2O]Cl_2	35–130	5.67 (4.86)	3.58x10^{7} (1.69x10^{7})	−12.00 (−11.20)	35.64 (34.83)	63.42 (63.81)
	130–260	14.31 (16.06)	4.32x10^{5} (6.35x10^{5})	−25.40 (−30.40)	142.7 (160.2)	180.0 (180.9)
	260–1000	11.73 (11.19)	4.46x10^{10} (2.31x10^{10})	−17.90 (−18.40)	116.8 (111.5)	204.0 (202.3)
[Fe(L)Cl]Cl_2.H_2O	30–335	5.86 (5.78)	3.87x10^{8} (2.79x10^{8})	−14.70 (−14.90)	58.40 (57.60)	77.21 (75.68)
	335–485	21.84 (23.26)	1.32x10^{6} (8.36x10^{6})	−28.90 (−32.50)	121.8 (123.2)	151.0 (152.0)
	485–890	41.79 (46.34)	6.32x10^{9} (1.76x10^{9})	−46.60 (−53.60)	144.7 (146.2)	186.1 (188.0)
[Co(L)Cl]Cl.H_2O	30–210	12.22 (11.43)	9.27x10^{7} (7.74x10^{7})	−30.50 (−29.70)	72.19 (74.00)	129. (127.8)
	210–350	23.74 (24.25)	1.80x10^{11} (2.49x10^{11})	−37.90 (−40.50)	93.69 (94.21)	121.8 (120.6)
	350–950	26.84 (26.75)	8.10x10^{5} (5.11x10^{5})	−38.80 (−40.10)	99.79 (98.67)	133.0 (134.2)
[Ni(L)Cl]Cl.H_2O	30–165	13.19 (13.24)	2.51x10^{9} (4.92x10^{9})	−32.60 (−34.20)	73.16 (73.22)	130.0 (129.0)
	165–255	14.85 (14.51)	5.64x10^{6} (6.97x10^{6})	−28.70 (−29.52)	64.81 (64.47)	122.3 (101.0)
	255–900	27.47 (28.77)	1.31x10^{6} (3.57x10^{8})	−47.50 (−51.60)	97.43 (98.73)	207.8 (207.9)
[Cu(L)H_2O]Cl_2.H_2O	40–205	15.68 (16.31)	7.50x10^{9} (9.47x10^{9})	−35.20 (−38.30)	75.64 (76.27)	149.0 (147.9)
	205–350	24.10 (23.83)	7.28x10^{8} (5.37x10^{8})	−43.20 (−44.20)	84.06 (83.79)	128.0 (130.2)
	350–1000	33.34 (32.97)	4.01x10^{7} (1.54x10^{7})	−48.50 (−49.60)	93.29 (93.86)	124.7 (124.2)
[Zn(L)Cl]Cl. H_2O	35–130	5.29 (5.37)	3.19x10^{8} (3.35x10^{8})	−12.20 (−13.70)	42.60 (43.40)	88.23 (89.75)
	130–340	22.26 (23.10)	8.46x10^{10} (1.20x10^{10})	−33.60 (−36.60)	72.21 (73.50)	122.2 (123.3)
	340–770	29.55 (30.62)	1.78x10^{7} (7.17x10^{7})	−41.40 (−44.50)	129.5 (130.6)	147.2 (147.9)
[Cd(L)Cl]Cl	30–270	10.82 (11.10)	6.52x10^{11} (7.40x10^{11})	−18.90 (−21.00)	78.12 (76.66)	118.0 (107.0)
	270–630	27.11 (23.31)	6.50x10^{7} (4.83x10^{7})	−42.10 (−37.93)	107.6 (108.7)	132.8 (132.0)

[#]The data between parenthesis are obtained using Horowitz-Metzger equation while the data without parenthesis are obtained using Coats-Redfern equation.

Where K_B is the Boltzmann constant, h is the Plank's constant and Ts is the DTG peak temperature.

(b) *Horowitz-Metzger equation*

The Horowitz-Metzger equation is an illustrative of the approximation methods. These authors derived the relation:

$$\log\left[\left(1-(1-\alpha)^{1-n}\right)/(1-n)\right] = \left(E^*\theta/2.303RT_g^2\right) \text{ for } n\neq 1$$

When $n = 1$, the LHS of equation 4 would be log[−log (1-α)]. For a first-order kinetic process the Horowitz-Metzger equation may be written in the form:

$$\log\left[\log\left(W_\alpha/W_\gamma\right)\right] = \left(E^*\theta/2.303RT_s^2\right) - \log 2.303$$

Where θ = T-Ts, $w_\gamma = w_\alpha - w$, w_α = mass loss at the completion of the reaction; w = mass loss up to time t. The plot of log[log(w_α /w_γ)] versus θ was drawn and found to be linear from the slope of which E* was calculated. The pre-exponential factor, A, was calculated from the equation:

$$\left(E^*/RT_s^2\right) = A/\left[\varphi\ \exp^{(-E^*/RTs)}\right]$$

The entropy of activation, ΔS*, enthalpy of activation, ΔH* and Gibbs free energy, ΔG*, were calculated using the following equations;

$$\Delta H^* = E^* - RT$$

$$\Delta G^* = \Delta H^* - T\Delta S^*$$

The activation energies of decomposition appeared in the range of 4.86–124.30 kJ mol^{-1}.[25,42] The positive sign of ΔG* for the investigated complexes revealed that the free energy of the final residue was higher than that of the initial compound, and all the decomposition steps were non-spontaneous processes. The values of the activation, ΔG* increased significantly for the subsequent decomposition stages of a given complex. This can be explained based on increasing the values of TΔS* significantly from one step to another overrides the values of ΔH*. On the other hand, the negative values of ΔS* for the degradation process showed more ordered activated complex than the reactants or the reaction was slow.[43,44]

3.9 | Structural interpretation

The general formula of metal ions complexes can be expected and illustrated in scheme 1, which were also confirmed by elemental analyses that show formation of complex in 1:1 ratio, molar conductance measurements show that all complexes are electrolytes, infrared

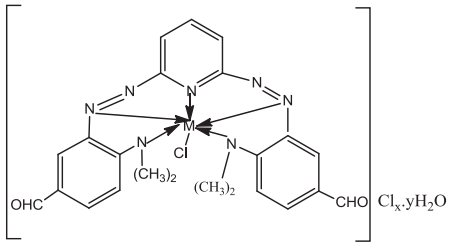

M = Cr(III), Fe(III); x = 2, y = 0
M = Co(II), Ni(II); x = 1, y = 1
M = Cd(II); x = 1, y = 0

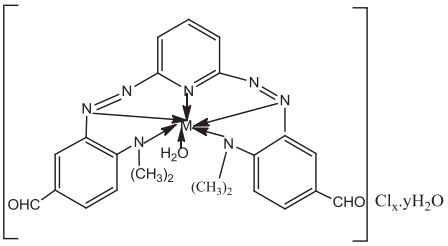

M = Mn(II), Zn(II); x = 2, y = 0
M = Cu(II); x = 2, y = 1

SCHEME 1 The proposed structures of different metal complexes

spectroscopy, UV–Vis, ^{1}H NMR and mass spectrometry all confirm complexes formation. On the basis of electronic spectral data and magnetic susceptibility measurements, octahedral geometry was proposed for metal complexes. X-ray diffraction study showed that the ligand, Cr(III) and Ni(II) complexes have crystalline, while other complexes have amorphous structures. The thermal stability of the ligand and its metal complexes was examined by thermogravimetry.

3.10 | Biological activities

The biological activities of the free ligand and its metal complexes were examined. A comparative study of the growth inhibition zone values of ligand and its metal complexes indicated that some metal complexes exhibited higher activity than the free ligand Table 7, Figure 4.

For *Bacillus subtilis* (gram positive bacteria): $[Zn(L)H_2O]Cl_2$ > $[Co(L)Cl]Cl.H_2O$ > [Cd(L)Cl]Cl > $[Ni(L)Cl]Cl.H_2O$ = $[Cu(L)H_2O]Cl_2.H_2O$ > $[Mn(L)H_2O]Cl_2$ > $[Fe(L)Cl]Cl_2$ = L > Amikacin > $[Cr(L)Cl]Cl_2$.

For *Staphylococcus aureus* (gram positive bacteria): $[Zn(L)H_2O]Cl_2$ = [Cd(L)Cl]Cl > $[Co(L)Cl]Cl.H_2O$ > $[Cu(L)H_2O]Cl_2.H_2O$ > $[Ni(L)Cl]Cl.H_2O$ > L = $[Cr(L)Cl]Cl_2$ = $[Mn(L)H_2O]Cl_2$ = $[Fe(L)Cl]Cl_2$ = Amikacin.

For *Escherichia coli* (gram negative bacteria): $[Co(L)Cl]Cl.H_2O$ = [Cd(L)Cl]Cl > $[Zn(L)H_2O]Cl_2$ > $[Ni(L)Cl]Cl.H_2O$ > $[Cu(L)H_2O]Cl_2.H_2O$ > L = $[Fe(L)Cl]Cl_2$ > $[Mn(L)H_2O]Cl_2$ > Amikacin > $[Cr(L)Cl]Cl_2$.

For *Neisseria gonorrhoeae* (gram negative bacteria): $[Zn(L)H_2O]Cl_2$ > [Cd(L)Cl]Cl > $[Cu(L)H_2O]Cl_2$.

TABLE 7 Biological activity of L and its metal complexes

	Inhibition zone diameter (mm / mg sample)				
	Gram positive		*Gram negative*		*fungus*
Sample	***Bacillus subtilis***	***Staphylococcus aureus***	***Escherichia coli***	***Neisseria gonorrhoeae***	***Candida albicans***
Control: DMSO	0	0	0	0	0
L	9	9	10	9	9
$[Cr(L)Cl]Cl_2.2H_2O$	0	9	0	0	0
$[Mn(L)H_2O]Cl_2$	10	9	9	0	0
$[Fe(L)Cl]Cl_2.H_2O$	9	9	10	10	0
$[Co(L)Cl]Cl.H_2O$	17	21	17	14	12
$[Ni(L)Cl]Cl.H_2O$	11	10	13	13	14
$[Cu(L)H_2O]Cl_2.H_2O$	11	13	12	16	9
$[Zn(L)Cl]Cl.H_2O$	20	28	15	26	0
[Cd(L)Cl]Cl	16	28	17	20	13
Amikacin	6	9	7	6	-
Ketokonazole	-	-	-	-	9

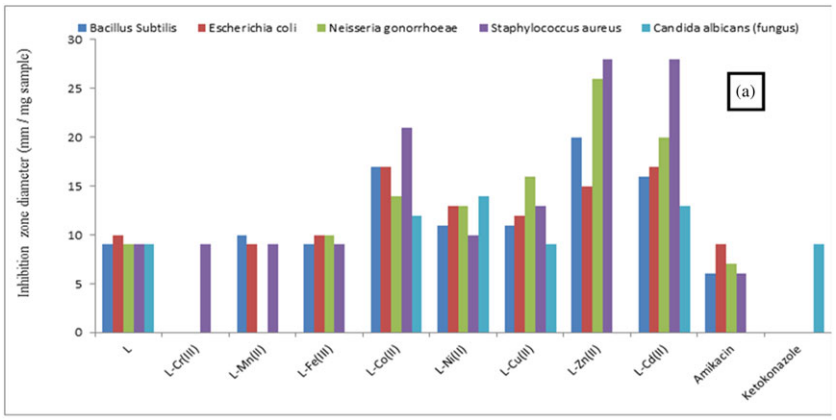

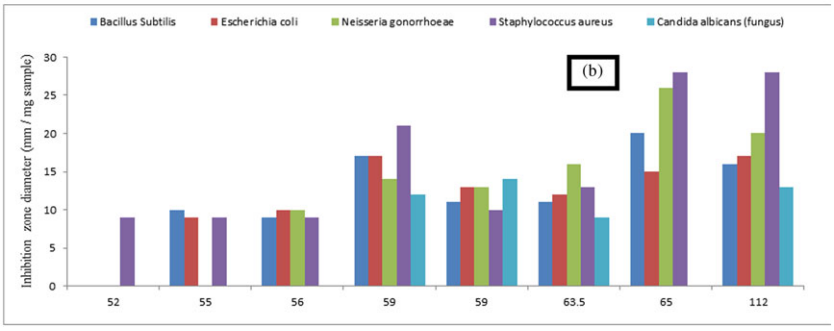

FIGURE 4 (a) Biological activity of azo dye ligand (L) and its complexes. (b) Relationship between inhibition zone diameter and atomic mass of metals

H_2O > $[Co(L)Cl]Cl.H_2O$ > $[Ni(L)Cl]Cl.H_2O$ > $[Fe(L)Cl]Cl_2$ > L > Amikacin > $[Cr(L)Cl]Cl_2$ = $[Mn(L)H_2O]Cl_2$.

For *Candida albicans* (fungus): $[Ni(L)Cl]Cl.H_2O$ > $[Cd(L)Cl]Cl$ > $[Co(L)Cl]Cl.H_2O$ > L = $[Cu(L)H_2O]Cl_2.H_2O$ = Ketokonazole > $[Cr(L)Cl]Cl_2$ = $[Mn(L)H_2O]Cl_2$ = $[Fe(L)Cl]Cl_2$ = $[Zn(L)H_2O]Cl_2$.

Higher activity of metal complex was probably due greater lipophilic nature of the complex. It increased activity of the metal complex, and can be explained on the basis of Overtone's concept and Tweedy's chelation theory.[45] According to Overtone's concept of cell permeability, the lipid membrane that surrounds the cell favours the

passage of only lipid soluble materials due to which liposolubility was considered to be an important factor that controls the antimicrobial activity. On chelation, the polarity of the metal ion will be reduced to a greater extent due to the overlap of the ligand orbital and partial sharing of positive charge of metal ion with donor groups. Further, it increases the delocalization of the π electrons over the whole chelate ring and enhances the lipophilicity of the complex. This increased lipophilicity enhances the penetration of the complexes into lipid membrane and thus blocks the metal binding sites on enzymes of microorganisms. These metal complexes also disturb the respiration process of the cell and thus block the synthesis of proteins, which restricts further growth of the organism.[10,13,45–49]

The activity indexes of the newly synthesized ligand and its metal complexes were calculated and plotted in figure (5) according to the following equation:

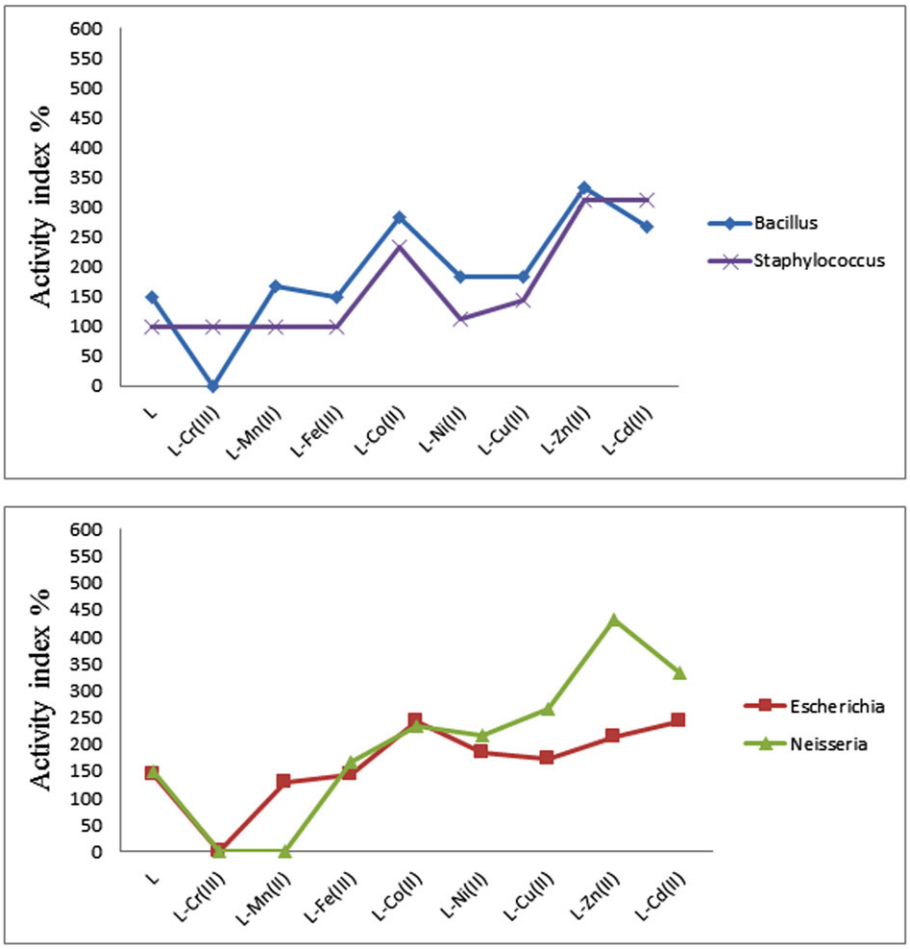

FIGURE 5 Activity index of azo dye ligand and its complexes against microbial organisms

TABLE 8 Antibreastic cancer activity of L and its metal complexes

Complex	Concn. (μg/ ml)	Surviving fraction (MCF7)					IC_{50} (μg/ ml)
		0.0	5.0	12.5	25.0	50.0	
L		1.00	0.97	0.71	0.76	0.43	44.50
$[Cr(L)Cl]Cl_2.2H_2O$		1.00	1.00	0.82	0.61	0.45	42.70
$[Co(L)Cl]Cl.H_2O$		1.00	0.80	0.72	0.53	0.29	28.00
$[Ni(L)Cl]Cl.H_2O$		1.00	0.91	0.76	0.76	0.48	47.90
$[Zn(L)Cl]Cl.H_2O$		1.00	0.85	0.62	0.47	0.46	22.60
[Cd(L)Cl]Cl		1.00	0.81	0.54	0.47	0.32	19.40

$$\text{Activity index(A)} = \frac{\text{Inhibition zone of compound(mm)}}{\text{Inhibition zone of standard drug(mm)}} \text{x } 100$$

The figures showed that Zn(II) complex has the highest activity index, while Cr(III) has no activity index against *Bacillus subtilis, Escherichia coli* and *Neisseria gonorrhoeae*.

3.10.1 | Anticancer activity evaluation:

The MCF7 cell line was chosen to study antibreastic cancer effect of the newly synthesized ligand and its metal ion complexes. The values of concentration at which half of the maximal effect is observed (IC_{50}) with the numerical data summarized in Table 8. Figure 6 showed relation between surviving fraction and concentration of compounds under investigation. It was clear from Table 8 that the free ligand has IC_{50} value of 44.5 μg/ml, while Cr(III), Co(II), Ni(II), Zn(II) and Cd(II) complexes have IC_{50} in the range of 19.4–47.9 μg/ml. the highest IC_{50} value was of Ni(II) complex (47.9 μg/ml), the lowest value was of Cd(II) complex (19.4 μg/ml), this means that Cd(II) complex had very high cytotoxic activity against MCF-7 cell line. These results provided a perfect example of how changes in the chelation molecular structure could lead to profound differences in anticancer activity.[50–52]

3.11 | Binding to biological macromolecules

DNA is considered a major biological target for compounds that have pharmacological activity. These compounds are a well-known for cancer chemotherapy.[53] We have computationally investigated the reaction between the azo ligand (L) and two macromolecules (MMs). The calculated structure of L was docked with two possible biological targets: the receptors of nucleoside diphosphate kinase of *Staphylococcus aureus* (PDB code: 3Q8U), and breast cancer mutant oxidoreductase (PDB code: 3HB5). The structures of these MMs were obtained from the Protein Data Bank. Table 9 contains the calculated binding energies for the interaction with these MMs. Generally, the azo ligand demonstrated strong binding interactions with two investigated proteins as demonstrated by the significantly negative binding energies computed in each case. It was observed that the azo ligand bound stronger to 3Q8U than to 3HB5 with a low binding energy −3.3 kcal/mol. Representative binding

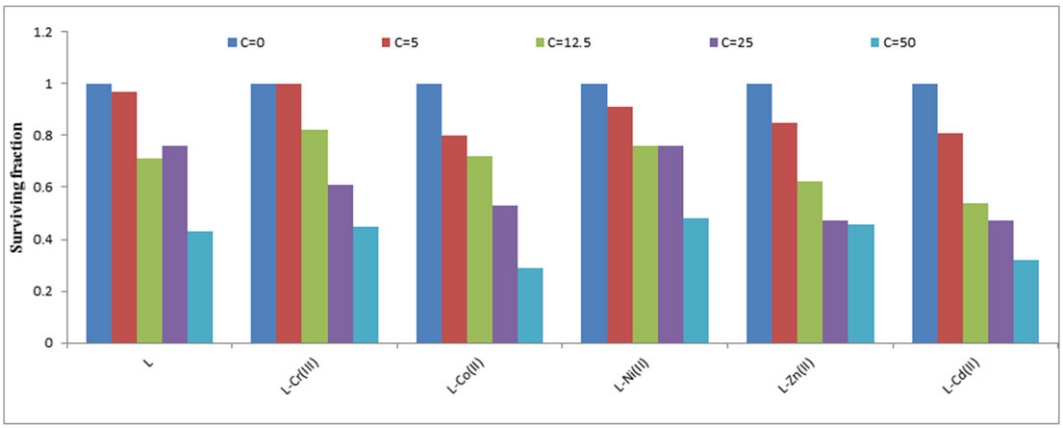

FIGURE 6 Anticancer activity of azo dye ligand and its complexes

TABLE 9 Energy values obtained in docking calculations of L with receptors of crystal structure of breast cancer mutant 3HB5-oxidoreductase and crystal structure of *S. aureus* (3Q8U)

Receptor	Ligand moeity	Receptor site	Interaction	Distance (A°)	E (kcal/mol)
3HB5	O 56	N MET 193	H-acceptor	2.92	−0.8
	6-ring	CD1 ILE 14	pi-H	3.78	−0.8
	6-ring	CD2 PHE 192	pi-H	3.65	−0.7
3Q8U	N 12	N THR 91	H-acceptor	3.30	−0.1
	O 55	NH1 ARG 125	H-acceptor	3.18	−3.3
	6-ring	NH1 ARG 85	pi-cation	3.96	−0.7
	6-ring	N THR 91	pi-H	4.38	−1.1

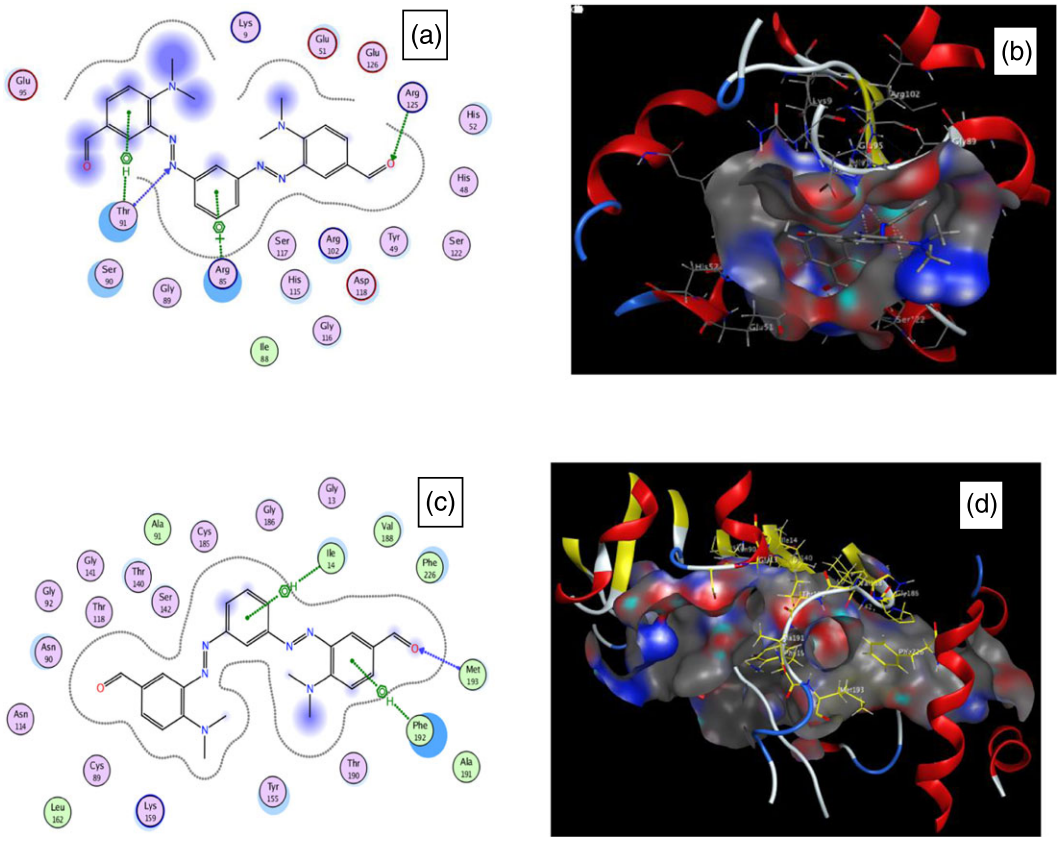

FIGURE 7 The interaction between i) [L and receptor 3Q8U (a) 2D plot, (b) 3D plot] and ii)[L and receptor 3HB5 (c) 2D plot and (d) 3D plot]

poses for the azo ligand revealed the strongly favorable affinities to be a consequence of extensive hydrophobic interactions with binding site residues Figure 7.

4 | CONCLUSION

In this work, a new free azodye ligand was prepared by coupling diazotized 2,6-diaminopyridine with p-dimethylaminobenzaldehyde then a series of metal ions complexes were synthesized. The free ligand and its complexes were characterized using different techniques. Elemental analysis showed that formation of ligand:metal in ratio 1:1. IR analysis confirmed coordination of ligand to metal via pyridine nitrogen, azo nitrogen and tertiary amine nitrogen also ^{1}HNMR confirmed that. Mass spectrometry showed molecular ion peak as the expected molecular weight. Conductivity measurements showed that all metal complexes are electrolytes. The magnetic and solid reflectance measurements confirmed octahedral geometry of the complexes, and XRD results showed that the free ligand, Cr(III) and Ni(II) complexes have crystalline structure while other complexes have amorphous nature. ESR spectra of solid Cu(II) complex at room temperature showed axial type (dx_2-y_2) with covalent bond character in an octahedral environment.

The proposed metal ions complexes structures as follow:

$$[MLCl]Cl_x.yH_2O \text{ where } M = Cr(III),\ Fe(III);$$

$$x = 2, y = 0, M = Co(II), Ni(II);$$

$$x = 1, y = 1 \text{ and } M = Cd(II);$$

$$x = 1, y = 0.[ML(H_2O)]Cl_x.yH_2O$$

$$\text{where } M = Mn(II), Zn(II); x = 2, y = 0 \text{ and}$$

$$M = Cu(II); x = 2, y = 1.$$

The antimicrobial studies showed that most metal ions complexes have higher activity than the free ligand.

The antibreastic cancer test showed that Ligand and complexes have high IC_{50} but Ni(II) complex showed the highest IC_{50} (47.90 μg/ ml). The docking study with two different proteins provided useful structural information for inhibition studies of free azo ligand.

ORCID

Walaa H. Mahmoud http://orcid.org/0000-0001-9187-4325

REFERENCES

[1] E. O. M. Rufchahi, A. G. Gilani, *Dyes Pig. J.* **2012**, *95*, 632.

[2] S. Menati, A. Azadbakht, R. Azadbakht, A. Taeb, A. Kakanejadifard, *Dyes Pig. J.* **2013**, *98*, 499.

[3] G. U. Prashant, V. S. Patil, V. S. Padalkar, K. R. Phatangare, V. D. Gupta, A. B. Thate, N. Sekar, *Dyes Pigments J.* **2013**, *99*, 291.

[4] K. Nejati, Z. Rezvani, B. Massoumi, *Dyes Pigments J.* **2007**, *75*, 653.

[5] F. Karcı, *Chem. Hetero. Compd. J.* **2013**, *3*, 492.

[6] J. Geng, Y. Dai, H.-F. Qian, W. Na Wang, *Huang, Dyes and Pigments J.* **2015**, *117*, 133.

[7] G. Hussain, M. Ather, M. Khan, A. Saeed, R. Saleem, G. Shabir, B. Channar, *Dyes Pigment J.* **2016**, *130*, 90.

[8] V. T. Kasumo, *Spectrochim. Acta A J.* **2001**, *57*, 1649.

[9] S. M. Annigeri, M. Sathisha, V. Revankar, *J. Coord. Chem.* **2008**, *61*, 4011.

[10] H. F. Abd El-Halim, G. G. Mohamed, M. M. I. El-Dessouky, W. H. Mahmoud, *Spectrochim Acta A J.* **2011**, *82*, 8.

[11] M. J. Frisch, G. W. Trucks, H. B. Schlegel, G. E. Scuseria, M. A. Robb, J. R. Cheeseman, V. G. Zakrzewski, J. A. Montgomery, R. E. Stratmann, J. C. Burant, S. Dapprich, J. M. Millam, A. D. Daniels, K. N. Kudin, M. C. Strain, O. Farkas, J. Tomasi, V. Barone, M. Cossi, R. Cammi, B. Mennucci, C. Pomelli, C. Adamo, S. Clifford, J. Ochterski, G. A. Petersson, P. Y. Ayala, Q. Cui, K. Morokuma, D. K. Malick, A. D. Rabuck, K. Raghavachari, J. B. Foresman, J. Cioslowski, J. V. Ortiz, A. G. Baboul, B. B. Stefanov, G. Liu, A. Liashenko, P. Piskorz, I. Komaromi, R. Gomperts, R. L. Martin, D. J. Fox, T. Keith, M. A. Al-Laham, C. Y. Peng, A. Nanayakkara, C. Gonzalez, M. Challacombe, P. M. W. Gill, B. G. Johnson, W. Chen, M. W. Wong, J. L. Andres, M. Head-Gordon, E. S. Replogle, J. A. Pople, *GAUSSIAN 03 (Revision A.9)*, Gaussian, Inc., Pittsburgh **2003**.

[12] Molecular Operating Environment (MOE 2008.10), Chemical Computing Group Inc., Montreal, QC, Canada.

[13] N. A. El-Ghamaz, A. Z. El-Sonbati, M. A. Diab, A. A. El-Bindary, G. G. Mohamed, S. M. Morgan, *Spectrochim. Acta A* **2015**, *430*, 96.

[14] W. H. Mahmoud, G. G. Mohamed, M. M. I. El-Dessouky, *Int. J. Electrochem. Sci.* **2014**, *9*, 1415.

[15] S. Chandra, Vandana, S. Kumar, *Spectrochim. Acta A J.* **2015**, *135*, 356.

[16] W. H. Mahmoud, N. F. Mahmoud, G. G. Mohamed, **AOC J.**, Accepted: 23 **March 2017**

[17] N. A. El-Ghamaz, A. Z. El-Sonbati, M. A. Diab, A. A. El-Bindary, M. K. Awad, S. M. Morgan, *Mater. Sci. Semicond. Process. J.* **2014**, *9*, 150.

[18] W. H. Mahmoud, N. F. Mahmoud, G. G. Mohamed, A. A. El-Bindary, A. Z. El-Sonbati, *J. Mol. Struct.* **2012**, *1086*, 266.

[19] A. Z. El-Sonbati, M. A. Diab, A. A. El-Bindary, A. M. Eldesoky, S. M. Morgan, *Spectrochim. Acta A* **2015**, *135*, 774.

[20] N. A. El-Ghamaz, M. A. Diab, A. A. El-Bindary, A. Z. El-Sonbati, H. A. Seyam, *J. Mater. Sci. Semicond. Proc.* **2014**, *27*, 521.

[21] F. A. Beckford, A. Brock, A. Gonzalez-Sarras, N. P. Seeram, *Mol. Str. J.* **2016**, *1121*, 156.

[22] S. Altürk, D. Avcı, M. Tamer, Y. Atalay, O. Şahin, *Phys. Chem. Solids* **2016**, *98*, 71.

[23] D. Choi, L. Geum-Sook, Y. L. Piao, C. On-You, C. Ki-An, P. Choon-Bae, C. Young-Cheol, S. Young-Il, L. Myung-Koo, H. Cho, *Korean J. Chem. Eng.* **2014**, *31*, 2221.

[24] A. A. Abou-Hussein, W. Linert, *Spectrochim. Acta A 117*, 763.

[25] S. Ilhan, H. Temel, I. Yilmaz, A. Kilic, *Transition Met. Chem.* **2007**, *32*, 344.

[26] A. Kakanejadifard, F. Azarbani, A. Zabardasti, S. Kakanejadifard, M. Ghasemian, F. Esna-ashari, S. Omidi, S. Shirali, M. Rafieefar, *Dyes Pig. J.* **2013**, *97*, 215.

[27] W. H. Mahmoud, G. G. Mohamed, M. M. I. El-Dessouky, *Mol. Str. J.* **2015**, *1082*, 12.

[28] W. H. Mahmoud, R. G. Deghadi, G. G. Mohamed, *Res. Chem. Intermed.* **2016**, *5*, 42.

[29] W. H. Mahmoud, R. G. Deghadi, G. G. Mohamed, *Appl. Organomet. Chem.* **2016**, *30*, 221.

[30] F. A. Cotton, G. Wilkinson, C. A. Murillo, M. Bochmann, *Advanced Inorganic Chemistry*, 6th ed., Wiley, New York **1999**.

[31] S. H. Etaiw, D. M. Abd El-Aziz, E. H. Abd El-Zaher, E. A. Ali, *Spectrochim. Acta A* **2011**, *79*, 1331.

[32] M. Tyagi, S. Chandra, P. Tyagi, *Spectrochim. Acta A* **2014**, *117*, 1.

[33] P. Tyagi, S. Chandra, B. S. Saraswat, D. Yadav, *Spectrochim. Acta A* **2015**, *15*, 155.

[34] M. Popescu, P. Rotaru, M. Bubulica, A. Kriza, *J. Therm. Anal. Calorim.* **2015**, *120*, 641.

[35] A. W. Coats, J. P. Redfern, *Nature* **1964**, *201*, 68.

[36] G. G. Mohamed, E. M. Zayed, A. M. M. Hindy, *Spectrochim Acta A.* **2015**, *145*, 76.

[37] M. Asadi, S. Torabi, K. Mohammadi, *Spectrochim. Acta A* **2014**, *122*, 676.

[38] O. A. El-Gammal, M. M. Bekheit, M. Tahoon, *Spectrochim. Acta A* **2015**, *135*, 597.

[39] D. K. Demertzi, P. N. Yadav, J. Wiecek, S. Skoulika, T. Varadinova, M. A. Demertzis, *J. Inorg. Biochem.* **2006**, *100*, 1558.

[40] M. Belicchi-Ferrari, F. Bisceglie, G. Pelosi, P. Tarasconi, *Polyhedron* **2008**, *27*, 1361.

[41] H. W. Horowitz, G. Metzger, *Anal. Chem.* **1963**, *35*, 1464.

[42] A. A. Frost, R. G. Pearson, *Kinetics and Mechanism*, Wiley, New York **1961**.

[43] O. A. El-Gammal, M. M. Bekheit, S. A. El-Brashy, *Spectrochim. Acta A* **2015**, *137*, 207.

[44] T. Hatakeyama, F. X. Quinn, *Thermal Analysis Fundamentals and Applications to Polymer Science*, 2nd ed., Wiley, Chichester **1994**.

[45] K. Kralova, K. Kwassova, O. Svajlenova, J. Vanco, *Chem. Pap.* **2000**, *58*, 361.

[46] A. Z. El-Sonbati, M. A. Diab, A. A. El-Bindary, G. G. Mohamed, S. M. Morgan, *Inorg. Chim. Acta* **2015**, *430*, 96.

[47] S. Chandra, S. Gautam, H. K. Rajor, R. Bhatia, *Spectrochimica Acta A*, Accepted Date: 24 August **2014**, https://doi.org/10.1016/j.saa.2014.08.046.

[48] A. T. C. Olak, F. C. Olak, O. Z. Yesilel, D. Akduman, F. Yilmaz, M. Tümer, *Inorg. Chim. Acta* **2010**, *363*, 2149.

[49] S. Belaid, A. Landreau, S. Djebbar, O. B. Baitich, G. Bouet, J. P. Bouchara, *J. Inorg. Biochem.* **2008**, *102*, 63.

[50] J. Pwerekh, P. Inamdhar, R. Nair, S. Baluja, S. Chand, *J. Serb. Chem. Soc. J.* **2005**, *70*, 1161.

[51] Y. Vaghasia, R. Nair, M. Soni, S. Baluja, S. Chand, *J. Serb. Chem. Soc. J.* **2004**, *69*, 991.

[52] N. Raman, *Res. J. Chem. Enviro.* **2005**, *4*, 9.

[53] W. H. Mahmoud, F. N. Sayed, G. G. Mohamed, Accepted: 29 April **2016**. https://doi.org/10.1002/aoc.3529.

How to cite this article: Mahmoud WH, Sayed FN, Mohamed GG. Azo dye with nitrogen donor sets of atoms and its metal complexes: Synthesis, characterization, DFT, biological, anticancer and Molecular docking studies. *Appl Organometal Chem*. 2018;e4347. https://doi.org/10.1002/aoc.4347